Journal of Computational Science and Technology

Vol. 2, No. 2, 2008

An Improved Lattice Boltzmann Model for Immiscible Fluids*

Long WU**, Michihisa TSUTAHARA** and Shinsuke TAJIRI**

** Graduate School of Science and Technology, Kobe University

1-1 Rokko-dai, Nada-ku, Kobe, Japan

E-mail: tutahara@mech.kobe-u.ac.jp

Abstract

We proposed an improved immiscible lattice BGK model for simulating multiphase flows. The surface tension effect was recovered by introducing a force term based on the appropriate continuum physics. The anti-diffusion scheme in the mixed region was applied to reduce the side-effect of recoloring step and control the thickness of the interface. The simulation of a static bubble was used as a test case. Laplace's law, spurious velocities and isotropy property were examined. The results show that our model has more advantages for simulations of immiscible fluids over the existing immiscible lattice BGK models. Furthermore, the simulations of droplet formation in a Cross-junction microchannel were performed and compared with the experiments. The numerical results show good agreements with the experimental ones for the evolution of the droplet.

Key words: Lattice Boltzmann Method, Multiphase Flow, Immiscible Fluids, Interfacial Tension, Droplet Formation

1. Introduction

In recent years, the lattice Boltzmann (LB) method has developed into an alternative and powerful tool of computational fluid dynamics, especially for complex fluids[(1)]. One particular application of the lattice Boltzmann method, which has attracted considerable attention, is the modeling of inhomogeneous fluids, such as immiscible multiphase flow [(2)-(13)]. These flows are difficult to be simulated by conventional techniques of solving the Navier-Stokes equations. The main difficulty of conventional method comes from the microscopic mechanism of interfaces. However, this physics can be inserted into the model by some intuitive ways as illustrated in several fluid-fluid interface generating techniques developed from the basic LB model. There are several LB models for the simulation of multiphase flow. The first immiscible LBGK model (ILBGK) was proposed by Gunstensen *et al*[(3)(4)] based on R-K lattice gas model[(2)] and modified by Grunau *et al*[(5)]. Two kinds of colored particles (red and blue) are introduced for two phases. The local flux and color field (color gradient) are calculated and the maximum work of color flux against the color field is chosen to encourage the preferential grouping of same colors. Perturbation step was introduced to realize the surface tension effect. This model retains sharp interfaces and the surface tension in this model may be calculated analytically by setting a single adjustable parameter. An alternative multiphase LB model proposed by Shan and Chen[(6)-(9)] is based on microscopic interactions. This model also has sharp interfaces and allows the simulations of two phases with significantly different densities in the case of one component fluid. Both models have unphysical properties and the inconsistency between thermodynamic and kinetic pressure[(13)]. In the Shan and Chen model, the surface tension is given by the strength of the microscopic interactions and the shape of the density profile at the liquid-gas

*Received 1 Feb., 2008 (No. 08-0056)
[DOI: 10.1299/jcst.2.307]

interface. Although it is possible to adjust these two, keeping the density profile constant and changing the surface tension requires the adjustment of two parameters independently. Furthermore, the absolute value of surface tension is not known prior to evaluation of the density profile at the interface. The third LB model of multiphase flow was proposed by Swift *et al*[10][11] using a free-energy approach. Their model is constructed so that the pressure tensor is consistent with the one derived from the free-energy function of nonuniform fluid. This model leaves the interface relatively wide. There also exists a class of LB models that are derived from kinetic equations[12][13]. These models can simulate two-phase miscible and immiscible fluid flow depending upon the choice of the inter-particle interactions.

All of the above models have their positive and negative properties. To use one model instead of others is a question of the taste and of the application of interest. Here we study a modified version of the first immiscible LB model (LBGK) for two reasons. Firstly, the sharp interface is maintained and hence the position of the interface can be known accurately; secondly, this is the only technique that allows to separate the treatment of surface tension effects from interface tracking, so that the value of the surface tension is easy to be calculated and adjusted. Although, both properties are advantageous when studying complex interface motion in confined and/or complex geometries, it should be noted that the immiscible model still has some unphysical properties, such as spurious velocities near interface and side-effect of distributing the interface. In the present work, we focus our attention on these problems and try to propose a more reasonable immiscible LBGK model.

2. Numerical method

In this section, the original immiscible lattice BGK model (Gunstensen model[3]) will be reviewed briefly, and a more reasonable variation will be given in detail.

2.1 Gunstensen's original model

Gunstensen gave the first immiscible lattice BGK model for multiphase flow. The two fluids denoted by different colors, red and blue, obey the lattice Boltzmann equation as:

$$f_i^k\left(\mathbf{x}+\mathbf{e}_i,t+1\right)-f_i^k\left(\mathbf{x},t\right)=\Omega_i^k\left(\mathbf{x},t\right) \tag{1}$$

where, $f_i^k\left(\mathbf{x},t\right)$ is the particle distribution in the i-th velocity direction for the k-th fluid (red or blue) at the position $\mathbf{x}$ and time t. These particle distributions are evolved by Eq.(1). The collision operator, $\Omega_i^k\left(\mathbf{x},t\right)$, can be split into two parts. The first part denoted by $\left(\Omega_i^k\right)^1$ is the same as the BGK single-phase collision term and can be simplified as:

$$\left(\Omega_i^k\right)^1=-\frac{1}{\tau_k}\left[f_i^k\left(\mathbf{x},t\right)-f_i^{k(eq)}\left(\mathbf{x},t\right)\right] \tag{2}$$

where, $f_i^{k(eq)}\left(\mathbf{x},t\right)$ is the equilibrium distribution at position $\mathbf{x}$ and time t, and τ_k is the single-relaxation time for the kth fluid. The second part of the collision operator for the 2-D 7-speed model is given as:

$$\left(\Omega_i^k\right)^2=A\left|\mathbf{G}\right|\cos 2\left(\theta_i-\theta_f\right) \tag{3}$$

where, A is the adjustable surface tension parameter, θ_i is the angle of lattice direction i, and θ_f is the angle of local gradient of color field $\mathbf{G}$ which is defined as:

$$\mathbf{G}\left(\mathbf{x},t\right)=\sum_i \mathbf{e}_i\left[\rho_r\left(\mathbf{x}+\mathbf{e}_i,t\right)-\rho_b\left(\mathbf{x}+\mathbf{e}_i,t\right)\right] \tag{4}$$

To prevent both phases from mixing with each other, the so-called recoloring step is applied. The basic idea of recoloring is to keep the interface sharp by reallocating $f_i^k\left(\mathbf{x},t\right)$ in the mixed region at collision step, so that as few as possible colored particles crosses the

interface. The colored particles are demixed relative to the color field **G** by maximizing the work done by color the flux $\mathbf{q}(\mathbf{x},t)$,

$$\mathbf{q}(\mathbf{x},t)=\sum_i \mathbf{e}_i\left[f_i^r(\mathbf{x},t)-f_i^b(\mathbf{x},t)\right] \tag{5}$$

Because of this "recolor" procedure, particles of one color tend to congregate together. Thus, the two fluids are forced to be immiscible in this model.

2.2 Present method

We now modify the Gunstensen model by replacing the perturbation step with a direct force term at the mixed site, and change the recoloring step by including moderate diffusion between different phases.

With the same notation, the lattice Boltzmann equation for the *k*th component can be written in the same form as Eq.(1), with the collision term as:

$$\Omega_i^k(\mathbf{x},t)=-\frac{1}{\tau_k}\left[f_i^k(\mathbf{x},t)-f_i^{k(eq)}(\mathbf{x},t)\right] \tag{6}$$

The 9-speed and 19-speed models are chosen in this study for two-dimensional and three-dimensional simulations, respectively. So that a suitable equilibrium distribution function takes the form

$$f_i^{k(eq)}=w_i\rho^k\left(1+3e_{i\alpha}u_\alpha+\frac{9}{2}e_{i\alpha}e_{i\beta}u_\alpha u_\beta-\frac{3}{2}\mathbf{u}^2\right) \tag{7}$$

where Greek letters α,β represent Cartesian co-ordinates and the summation convention are applied, and $w_0=4/9$, $w_i=1/9$ for $i=1,2,3,4$, $w_i=1/36$ for $i=5,6,7,8$ in two dimensional simulations and $w_0=1/3$, $w_i=1/18$, for $i=1...6$, $w_i=1/36$, for $i=7...18$ in three dimensional simulations.

In Eq.(6), τ_k is the relaxation time for each kind of fluid. It is used to decide the value of the kinematic viscosity as:

$$\nu=\frac{2\tau-1}{6} \tag{8}$$

where τ is the relaxation time for the color blind fluid and is defined as $\tau=\sum\rho^k\tau_k/\rho$.

The densities ρ^k for different phases, the total density ρ momentum $\rho\mathbf{u}$ and pressure p are obtained from the following equations

$$\rho^k=\sum_{i=0}^{N}f_i^k=\sum_{i=0}^{N}f_i^{k(eq)} \tag{9}$$

$$\rho=\sum_k\rho^k \tag{10}$$

$$\rho\mathbf{u}=\sum_{i=0}^{N}\mathbf{e}_i f_i=\sum_{i=0}^{N}\mathbf{e}_i f_i^{eq} \tag{11}$$

$$p=\frac{1}{3}\rho \tag{12}$$

In order to impose surface tension effect, Lishchuk[14] modified the Gunstensen's algorithm by replacing the perturbation step with a direct forcing term at mixed region to recover the required pressure difference across the interface. It has already been reported that the Lishchuk method provides much better drop's isotropy and reduces spurious velocities. The same idea was used in this study to improve the original Gunstensen model. The surface tension force **F** is included by CSF model[15]:

$$\mathbf{F} = \sigma\kappa \frac{\nabla C}{|\nabla C|} \tag{13}$$

where, σ is the surface tension coefficient. The color field $C(\mathbf{x},t)$ and interface curvature κ are given, respectively, as:

$$C(\mathbf{x},t) = \rho_r(\mathbf{x},t) - \rho_b(\mathbf{x},t) \tag{14}$$

$$\kappa = -(\nabla \cdot \hat{\mathbf{n}}) = \frac{1}{|\mathbf{n}|}\left[\left(\frac{\mathbf{n}}{|\mathbf{n}|}\cdot\nabla\right)|\mathbf{n}| - (\nabla\cdot\mathbf{n})\right] \tag{15}$$

where, $\hat{\mathbf{n}}(\mathbf{x})$ is the unit normal to the interface, and $\hat{\mathbf{n}}(\mathbf{x}) = \mathbf{n}(\mathbf{x})/|\mathbf{n}(\mathbf{x})|$. The normal vector $\mathbf{n}(\mathbf{x})$ is defined as:

$$\mathbf{n}(\mathbf{x}) = \nabla C(\mathbf{x}) \tag{16}$$

The two parts inside the bracket of Eq.(15) can be calculated as follows:

$$\begin{aligned}(\nabla\cdot\mathbf{n})_{i,j} &= \left(\frac{\partial n_x}{\partial x}\right)_{i,j} + \left(\frac{\partial n_y}{\partial y}\right)_{i,j} \\ &= \frac{1}{2\Delta x}\left[n_{x,i+1/2,j+1/2} + n_{x,i+1/2,j-1/2} - n_{x,i-1/2,j+1/2} - n_{x,i-1/2,j-1/2}\right] \\ &+ \frac{1}{2\Delta y}\left[n_{y,i+1/2,j+1/2} + n_{y,i-1/2,j+1/2} - n_{y,i+1/2,j-1/2} - n_{y,i-1/2,j-1/2}\right]\end{aligned} \tag{17}$$

the normal vector $\mathbf{n}_{i,j}$ on the grid point and cell centered $\mathbf{n}_{i+1/2,j+1/2}$ are calculated by the following equations

$$\mathbf{n}_{i,j} = \frac{1}{4}\left(\mathbf{n}_{i+1/2,j+1/2} + \mathbf{n}_{i+1/2,j-1/2} + \mathbf{n}_{i-1/2,j+1/2} + \mathbf{n}_{i-1/2,j-1/2}\right) \tag{18}$$

$$\begin{aligned}\mathbf{n}_{i+1/2,j+1/2} &= \hat{\mathbf{x}}\left(\frac{C_{i+1,j} + C_{i+1,j+1} - C_{i,j} - C_{i,j+1}}{2\Delta x}\right) \\ &+ \hat{\mathbf{y}}\left(\frac{C_{i,j+1} + C_{i+1,j+1} - C_{i,j} - C_{i+1,j}}{2\Delta y}\right)\end{aligned} \tag{19}$$

The equilibrium distribution functions are the same as the ones given in Eq.(7) except the velocity $\mathbf{u}$ is replaced by the equilibrium velocity $\mathbf{u}^{eq}$, which is defined by the following relation:

$$\rho\mathbf{u}^{eq} = \rho\mathbf{u} + \tau\mathbf{F} \tag{20}$$

where, τ is the relaxation time for color blind fluid ($\tau = \sum_k(\rho_k\tau_k)/\sum_k\rho_k$).

The other improvement of our model is the modification of recoloring step by implementing Latva-Kokko's anti-diffusion scheme[16]. The crucial part of this solution is to allow the red and the blue fluid to moderately mix and to keep the color distribution symmetric with respect to the color gradient. We use the following redistributions for red and blue particle after collision step.

$$f_i^r = \frac{\rho_r}{\rho_r+\rho_b} f_i + \beta\frac{\rho_r\rho_b}{(\rho_r+\rho_b)^2} f_i^{eq(0)}\cos\varphi \tag{21}$$

$$f_i^b = \frac{\rho_b}{\rho_r+\rho_b} f_i - \beta\frac{\rho_r\rho_b}{(\rho_r+\rho_b)^2} f_i^{eq(0)}\cos\varphi \tag{22}$$

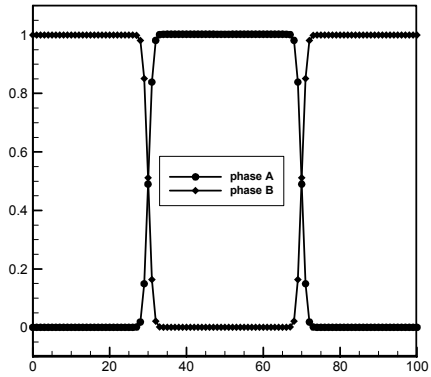

Fig.1 The interface profile at $\beta = 1$.

where, f_i and $f_i^{eq(0)}$ are the color-blind distribution functions and zero-velocity equilibrium distribution functions going to *i*th direction, respectively. φ, defined in Eq.(23), is the angle between the color gradient and the particle velocities $\mathbf{e}_i$. β is the parameter giving the tendency of the two fluids to separate.

$$\cos\varphi\big|_i = \frac{\mathbf{G}\cdot\mathbf{e}_i}{|\mathbf{G}||\mathbf{e}_i|} \tag{23}$$

Without the last term in the Eqs.(21) and (22), red and blue particles would be distributed according to their numbers and there would be no tendency for the separation of two fluids. Here, β can take any value between 0 and 1 to control the diffusion and width of interface. It should be noticed that when β is larger than 1, there can be negative populations of particles, but if the negative values are kept small, the stability is maintained. To avoid the negative distribution and keep sharp interface, β is set to be 1 in this paper. The profile of the two phases is shown in Fig.1 for $\beta = 1$.

3. Results and discussions

3.1 Validations of the current model

The usefulness of our new model for easily and accurately simulating multiphase flow is demonstrated by the case of a static circular bubble with radius R. Two dimensional (in the *xy*-plane) simulations were performed in a 100×100 lattice cell system. The periodic boundary conditions were employed.

First, we test Laplace's law, which is given as

$$\Delta P = P_{in} - P_{out} = \sigma/R \tag{24}$$

where, P_{in} and P_{out} are the average pressures inside and outside the bubble, respectively. Simulations with different initial bubble radii were performed, and the final radius *R* and the pressure differences were recorded. Figure 1 is the plot of $\Delta P = P_{in} - P_{out}$ versus $1/R$. Here, the value of σ is set to be 0.001. In Fig.2, all points representing a radius from 8 to 20 almost fit into a straight line. The pressure difference between inside and outside of the bubble is indeed proportional to the reciprocal of the radius in our simulations. This test shows that our method can correctly model the interfacial tension effect. In addition, it can be found that the slope ($\Delta P\cdot R = \sigma$) is quite close to the given interfacial tension σ. So, we can easily control the exact value of interfacial tension by the present method.

Second, the spurious velocities were examined for both the Gunstensen's model and the present model.

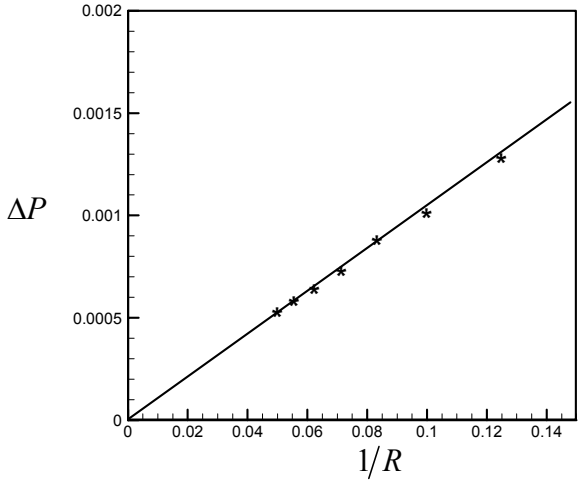

Fig.2 Numerical confirmation of Laplace's law by the present method.

Figure 3 shows velocity vectors at the final stage of bubble evolution for (a) Gunstensen's model and (b) the present model. The interfacial tension coefficient $\sigma = 0.001$ and the initial bubble radius R=15 are used for both models. Although there may be some small relative fluctuations as time evolves, they present the typical velocity field. The magnitude of the velocities is represented by the length of the velocity vectors (the reference length has the relation with grid size as (Grid units/magnitude=16000), for which the same scale is used in both models. The non-zero velocity fields in pictures (a) and (b) represent the deviation of the results from the physical problem, especially the velocities near the interface region. These non-zero velocities are called spurious velocities. It can be found that the spurious velocities are much more serious in the Gunstensen model (Fig.3 (a)) than the present model (Fig.3 (b)).

Third, the pressure distributions were investigated. Figure 4 shows the pressure distribution for (a) Gunstensen's model and (b) present model at $\sigma = 0.001$ and R=15. The same scale is used for both models. The anisotropy in our method, characterized by the pressure distribution, appears to be much smaller than that in the Gunstensen's model, as shown in Fig.4 (a) and (b). With the polar angle changing, the pressure distribution of our model almost keeps the same value as shown in Fig.4 (b), but Gunstensen's model (Fig.4 (a)) shows larger variation. The variation in pressure distribution may cause the anisotropy

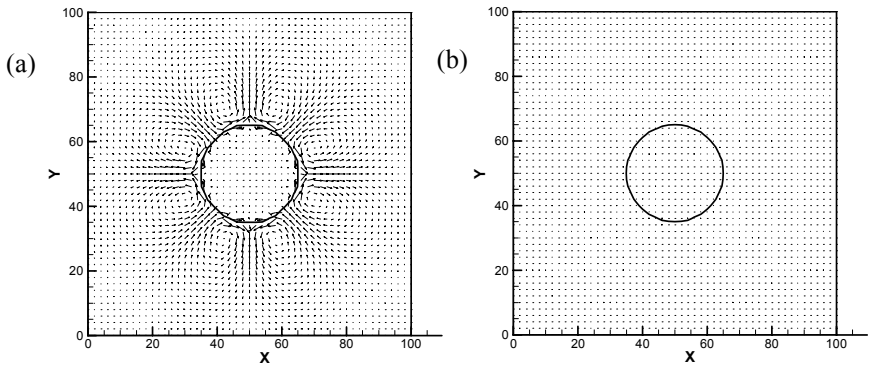

Fig.3 The distribution of velocity vectors at $\sigma = 0.001$ and $R = 15$ for (a) Gunstensen's model and (b) present model (Grid units (1.0) /reference magnitude=16000 for both models,).

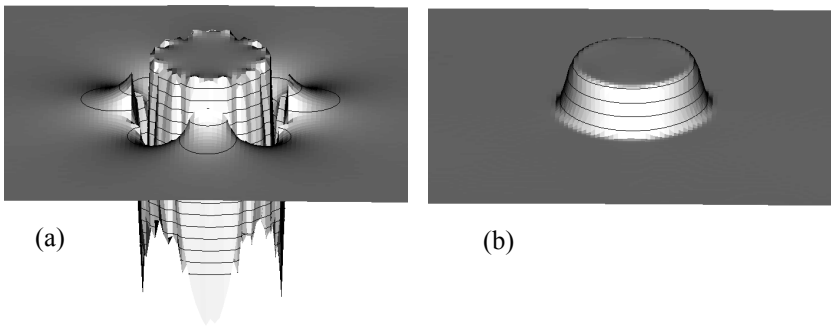

Fig.4 The pressure distribution at $\sigma = 0.001$ and $R = 15$ for (a) Gunstensen's model and (b) present model.

of bubble behavior and induce large spurious velocities. Besides, the present model obtains a continuous pressure distribution across the interface, while discontinuous distribution appears in Gunstensen's model.

3.2 Simulations of droplet formation in a Cross-junction microchannel

In the following, a more complex case (droplet formation in a Cross-junction microchannel) was studied by our new model. For this case, one challenge is the combination of low Reynolds number and Capillary number, which means that spurious velocities compare in magnitude to the modeled flow velocity. Therefore, to reduce the spurious velocities is very important for simulating this kind of problem accurately.

3.2.1 Model system

A cross-junction microchannel that had three inlet ports and single outlet was used in this study. This microchannel consisted of a main channel with a 200μm width and two lateral channels with 100μm widths as shown in Fig.5. The depth was 100μm through the whole channel. Fluid A (water-phase) was introduced into the main channel and fluid B (oil-phase) was injected into the lateral channels. As the water-phase, water with 3% PVA (viscosity, $\mu_A = 1.074\times10^{-2}\,\mathrm{Pa\cdot s}$; density, $\rho_A = 1.03\times10^{3}\,\mathrm{kg\cdot m^{-3}}$) was used. As the oil-phase, Freol ALPHA 10G (viscosity, μ_B=$2.441\times10^{-2}\,\mathrm{Pa\cdot s}$; density, $\rho_B = 0.93\times10^{3}\,\mathrm{kg\cdot m^{-3}}$) was used. The interfacial tension coefficient is $\sigma = 0.03\mathrm{N\cdot m^{-1}}$. The magnitudes of the average inlet velocities are designated as u_A for the water and u_B

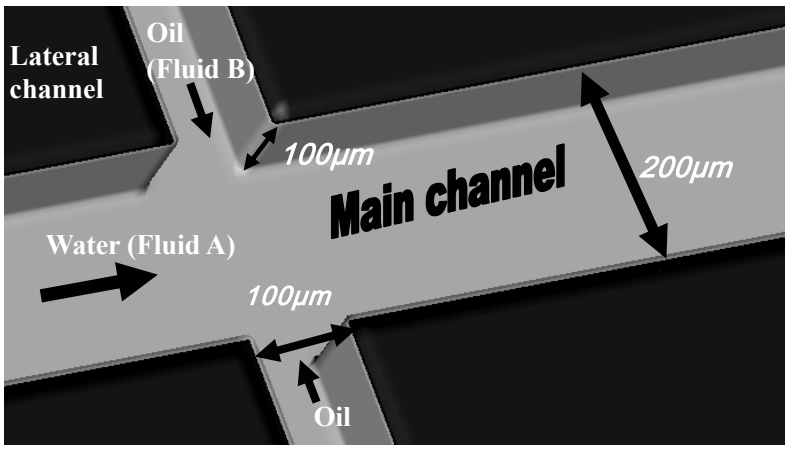

Fig.5 Model system for droplet formation in a Cross-junction microchannel.

for the oil. The velocity ratio is defined as $\alpha = u_A / u_B$.

Such flows are described by a large number of parameters including the interfacial tension, the inlet velocity, the viscosity and variations in the density across the two fluids. However, the Capillary number (*Ca*) which describes the relative importance of viscosity and interfacial tension always dominates such flow system. The Capillary number is defined as $Ca = \mu U / \sigma$ where μ is the viscosity, U is a typical velocity, and σ is the interfacial tension. In the current study, the comparisons between experiment and simulation are performed based on Capillary number.

Furthermore, several authors have reported the importance of the interaction between the fluids with the walls. In order to generate structures of one fluid (fluid A) within another fluid (fluid B), fluid B (oil-phase) usually completely wets the walls of the microchannel while fluid A (water-phase) is non-wetting. In this study, we also concentrate on the cases where only one fluid (fluid B) wets the walls. The same idea in article[17] is employed to realize the wetness effect.

3.2.2 Comparisons with experiments

Detailed comparisons were made between experiments and simulations for the evolution of the droplet formation (Here, experimental setup is not shown). In the simulations, the same values of viscosities, interfacial tension and inlet velocities as those in experiments were used. Therefore, same Capillary numbers were obtained for simulations and experiments. The slight difference in mass densities between the experimental solutions is neglected in the simulations. Here $\rho_A = 1.0$ $\rho_B = 0.0$ in phase A and $\rho_A = 0.0$ $\rho_B = 1.0$ in phase B are used for the initial conditions. The simulations are performed in a $301 \times 61 \times 11$ cubic cell system and each cell size corresponds to $10\mu m$. This cell system was tested to be acceptable by comparing the results of a finer cell system of $601 \times 121 \times 21$ (each cell size corresponds to $5\mu m$) in several different flow conditions. The relative error between the results of two cell systems is not more than 5%. No-slip boundary condition was applied for all the solid walls by the robust method of mid-link bounceback[18]. Inlet and outlet fluxes and an outlet pressure (density) distribution were specified at every time step using an appropriate equilibrium distribution function $f_i^{(0)}(\rho, \mathbf{u})$ [18].

Figure 6 shows a series of instantaneous states of droplet formation for (a) experimental results, (b) numerical results on x-y plane and (c) numerical results of 3D profiles. The inlet velocity of water (fluid A) is $u_A = 0.00084$ and the velocity ratio is $\alpha = 1/3$. The time moment and corresponding time steps are given for each picture. It can be found that the droplet shape and size in the simulation agree well with the experimental results. Droplet formation proceeds in three stages, i.e. expansion (i)-(iv), necking (v) and figuration (vi)-(vii). The final droplet size is a result of these three stages. In the simulation, the droplet detaches a little earlier than that in the experiment (v) and a little smaller droplet is obtained (vii). For both the experiment and the simulation, the necking stage happened very fast within about 2-3 ms. In this stage, the radius of the throat becomes very small and a strong interfacial tension force “cuts” the fluid A suddenly.

3.2.3 Influence of Capillary number on droplet size

Having validated the present model against experimental results, a series of simulations are performed at various interfacial tensions σ ($0.001 - 0.24$) for three different inlet velocities u_A ($0.00084, 0.00168, 0.00336$) at $\alpha = 1/3$. The viscosities used here for two fluids are $\mu_A = 0.01$ and $\mu_B = 0.024$ respectively. All above parameters appear in the Capillary number which is defined as $Ca = u_A \mu_A / \sigma$.

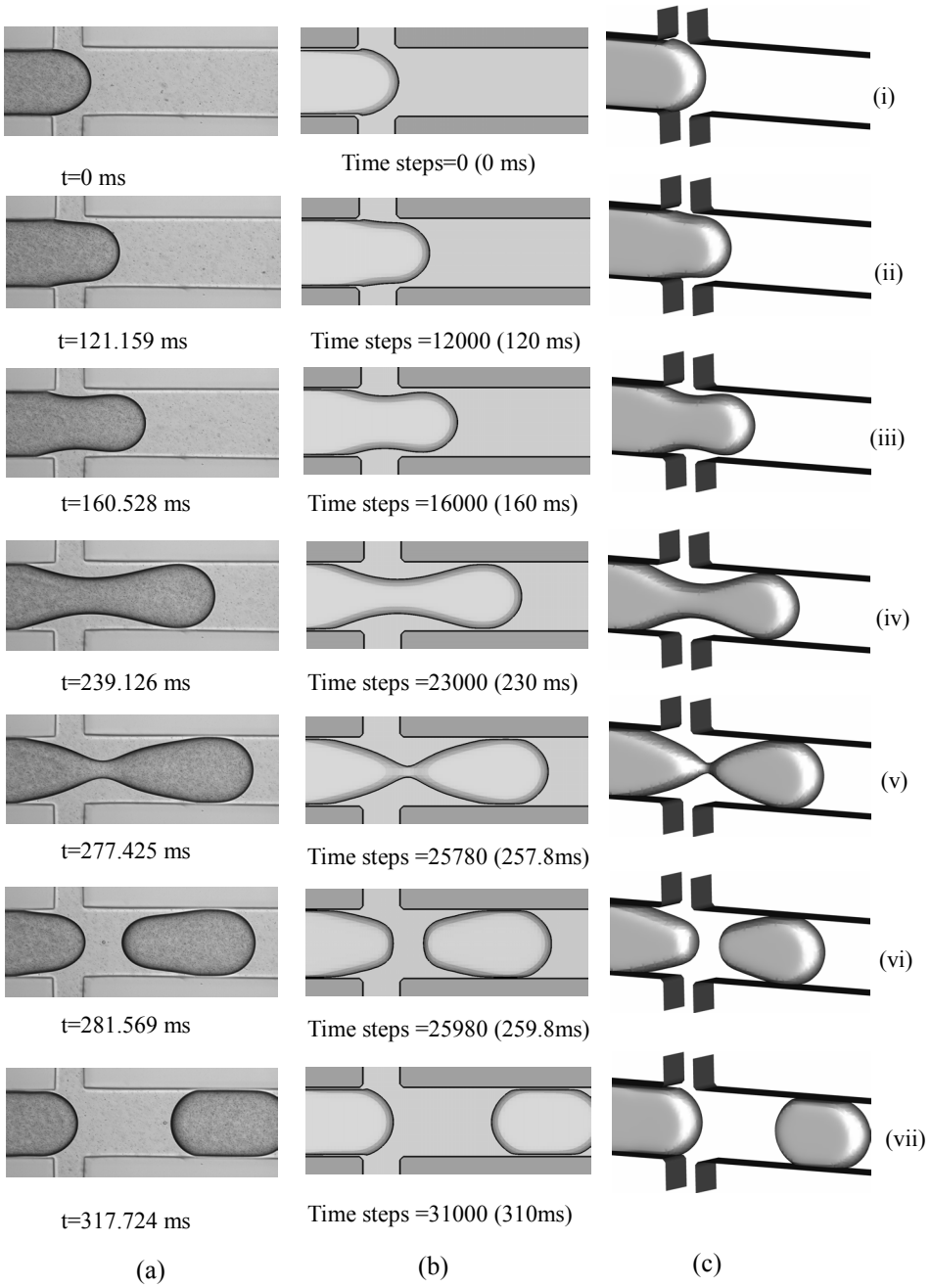

Fig.6 A series of instantaneous states of droplet formation for (a) experimental results, (b) numerical results on x-y plane and (c) numerical results of 3D profiles, at $u_A = 0.00084, Ca = 0.00028$ and $\alpha = 1/3$.

Figure 7 shows the plot of simulation results of relative droplet size (the droplet length divided by the width of the main channel) against the Capillary numbers. The corresponding values of parameters for each curve lines are given in Table 1. It can be found that three curve lines almost overlap when $Ca < 0.005$, although the Reynolds number and Weber number are different for each line. This proves that the flow mode is determined by the Capillary number at $Ca < 0.005$ predominantly. When the Capillary number reaches a large value ($Ca > 0.005$), three lines deviate from each other slightly and small droplets are generated under large inlet velocities. However, it seems that the flow is still determined by the Capillary number in general under the current conditions. Furthermore, the size of the generated droplet decreases when the Capillary number increases.

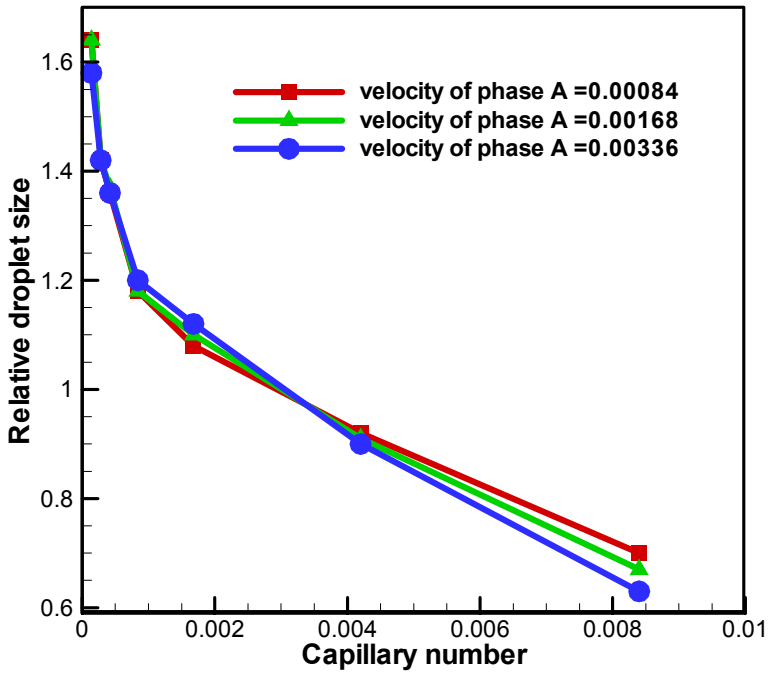

Fig.7 Simulation results of relative droplet size against various Capillary numbers under three different inlet velocities at $\alpha = 1/3$.

Table 1. The corresponding values of various parameters for Figure 7.

Ca \ u_A	0.00084	0.00168	0.00336
σ			
0.00014	0.06	0.12	0.24
0.00028	0.03	0.06	0.12
0.00042	0.02	0.04	0.08
0.00084	0.01	0.02	0.04
0.00168	0.005	0.01	0.02
0.0042	0.002	0.004	0.008
0.0084	0.001	0.002	0.004

4. Conclusions

An improved two-phase flow model has been proposed based on the Gunstensen model. The recoloring step of the original Gunstensen model was replaced by the anti-diffusion scheme, and the interfacial tension effect was recovered by introducing a direct force term which is deduced by CSF model. The present model has an advantage over the original Gunstensen model for depressing the spurious velocities and obtaining more reasonable pressure distribution across the interface. Three-dimensional simulations were carried out on the droplet formation in a Cross-junction microchannel using this model. Comparisons with experimental data were made and good results were obtained.

References

(1) Chen, S. and Doolen, G.D., Lattice Boltzmann Method for Fluid Flows, Annual Reviews of Fluid Mechanics, Vol.30. (1998), pp. 329-364.

(2) Rothman, D.H. and Keller, J.M., Immiscible Cellular-automaton Fluids, Journal of Statistical Physics, Vol.52, Nos.3/4 (1988), pp. 1119-1127.

(3) Gunstensen, A.K., Rothman, D.H., Zaleski, S., and Zanetti, G., Lattice Boltzmann Model of Immiscible Fluids, Physical Review A, Vol.43, No.8 (1991), pp. 4320-4327.

(4) Gunstensen, A.K. and Rothman, D.H., Microscopic Modeling of Immiscible Fluids in Three Dimensions by a Lattice Boltzmann Method, Europhysics Letters, Vol.18 (1992), pp. 157-161.

(5) Grunau, D., Chen, S., and Eggert, K., A Lattice Boltzmann Model for Multiphase Fluid Flows, Physics Fluids A, Vol.5, No.10 (1993), pp. 2557-2562.

(6) Shan, X. and Chen, H., Lattice Boltzmann Model for Simulating Flows With Multiple Phases and Components, Physical Review E, Vol.47, No.3 (1993), pp. 1815-1819.

(7) Shan, X. and Chen, H., Simulation of Nonideal Gases and Liquid-gas Phase Transitions by the Lattice Boltzmann Equation, Physical Review E, Vol.49, No.4 (1994), pp. 2941-2948.

(8) Shan, X. and Doolen, G.D., Multicomponent Lattice-Boltzmann Model with Interparticle Interaction, Journal of Statistical Physics, Vol.81 (1995), pp. 379-393.

(9) Shan, X. and Doolen, G.D., Diffusion in a Multicomponent Lattice Boltzmann Equation Model, Physical Review E, Vol.54, No.4 (1996), pp. 3614-3620.

(10) Swift, M.R., Orlandini, E., Osborn, W.R., and Yeomans, J.M., Lattice Boltzmann Simulations of Liquid-gas and Binary Fluid Systems, Physical Review E, Vol.54, No.5 (1996), pp. 5041-5052.

(11) Swift, M.R., Osborn W.R., and Yeomans, J.M., Lattice Boltzmann Simulations of Nonideal Fluids, Physical Review letters, Vol.75, No.5 (1995), pp. 830-833.

(12) Luo, L.-S., Unified Theory of Lattice Boltzmann Models for Nonideal Gases, Physical Review letters, Vol.81,No.8 (1998), pp. 1618-1621.

(13) Luo, L.-S., Theory of The Lattice Boltzmann Method: Lattice Boltzmann Models for Nonideal Gases, Physical Review E, Vol.62, No.4 (2000), pp. 4982-4996.

(14) Lishchuk, S.V., Care, C.M., and Halliday, I., Lattice Boltzmann Algorithm for Surface Tension with Greatly Reduced Microcurrents, Physical Review E, Vol.67 (2003), pp. 036701 1-5.

(15) Brackbill, J. U., Kothe, D. B. and Zemach, C., A Continuum Method for Modeling Surface Tension, Journal of Computational Physics, Vol.100, No.2 (1992), pp. 335-354.

(16) Latva-Kokko, M. and Rothman D.H., Diffusion Properties of Gradient-based Lattice Boltzmann Models of Immiscible Fluids, Physical Review E, Vol.71 (2005), pp. 056702 1-8

(17) Dupin, M.M., Halliday, I., Care, C.M., Simulation of a microfluidic flow-focusing device. Physical Review E 73 (2006), 055701 1-4.

(18) Succi S., The Lattice Boltzamnn Equation for Fluid Mechanics and Beyond, Oxford-Clarendon, Oxford, (2001).